

See discussions, stats, and author profiles for this publication at: <https://www.researchgate.net/publication/279230312>

Optimization of Broad-Response and High-Detectivity Polymer Photodetectors by Bandgap Engineering of Weak Donor–Strong Acceptor Polymers

ARTICLE *in* MACROMOLECULES · JUNE 2015

Impact Factor: 5.8 · DOI: 10.1021/acs.macromol.5b00859

READS

57

8 AUTHORS, INCLUDING:



Xiaokang Zhou

Chinese Academy of Sciences

13 PUBLICATIONS 39 CITATIONS

[SEE PROFILE](#)



Jidong Zhang

Chinese Academy of Sciences

101 PUBLICATIONS 1,106 CITATIONS

[SEE PROFILE](#)



Wenqiang Qiao

Chinese Academy of Sciences

32 PUBLICATIONS 354 CITATIONS

[SEE PROFILE](#)

Optimization of Broad-Response and High-Detectivity Polymer Photodetectors by Bandgap Engineering of Weak Donor–Strong Acceptor Polymers

Ji Qi,^{†,‡} Jinfeng Han,^{†,‡} Xiaokang Zhou,^{†,‡} Dezh Yang,[†] Jidong Zhang,[†] Wenqiang Qiao,^{*,†} Dongge Ma,[†] and Zhi Yuan Wang^{*,†,§}

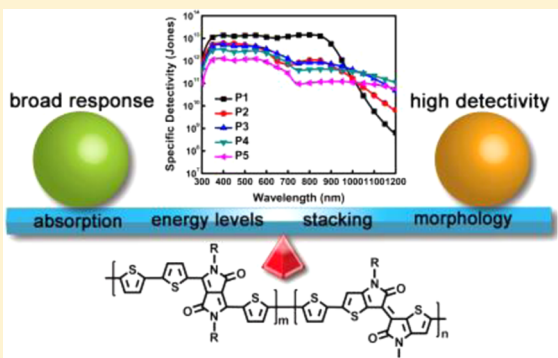
[†]State Key Laboratory of Polymer Physics and Chemistry, Changchun Institute of Applied Chemistry, Chinese Academy of Sciences, Changchun 130022, P. R. China

[‡]University of Chinese Academy of Sciences, Beijing 100049, P. R. China

[§]Department of Chemistry, Carleton University, 1125 Colonel By Drive, Ottawa, Ontario, Canada K1S 5B6

Supporting Information

ABSTRACT: A series of weak donor–strong acceptor polymers containing two different electron-deficient units (diketopyrrolopyrrole and thienoisoindigo) are synthesized and used in broad-response and high-detectivity polymer photodetectors. By adjusting the composition ratio of the two acceptors, the absorption spectra, energy levels, molecular stacking, and film morphology are affected, which in turn influence the photodetector performance. With increased thienoisoindigo component, the HOMO energy levels shift from -5.41 to -4.76 eV, and the LUMO energy levels are nearly unchanged, corresponding to reduced bandgaps and red-shifted absorption spectra. 1,8-Diodooctane additive shows greatly impact on the film morphology, which affects the photodetector performance significantly. Going from **P1** to **P5**, the detectivity decreases, but the response range increases. The photodetector based on **P4** exhibits detectivity of greater than 10^{11} Jones in a broad spectral region of 300–1200 nm, which is really promising for UV–vis–NIR light detection.



INTRODUCTION

Sensing the optical signals from ultraviolet–visible (UV–vis) to near-infrared (NIR) spectral region or panchromatic photo-detection is essential for various applications, such as full color imaging, optical communication, night-time surveillance, and environmental monitoring.^{1–5} Polymer photodetectors have been explored as attractive candidates for panchromatic detection as they possess a number of intrinsic merits such as flexibility, light weight, low cost, easy fabrication, and large material varieties.^{6–10} These unique features make polymer photodetector a promising replacement or complementarity to its inorganic counterpart, for example, the commercially available silicon photodetector, which is commonly used for UV–vis–NIR light detection in the spectral region of 400–1100 nm. However, technical challenges remain for polymer photodetectors to compete with silicon photodetectors in terms of spectral response and detectivity.^{11–14} One of the most urgent issues to be addressed is the lack of low-bandgap polymers with good photovoltaic response beyond 1100 nm. In-depth investigation and comprehensive understanding of the structure–property relationships of low-bandgap polymers should guide further development of panchromatic polymer photodetectors.

For organic semiconductors, the response spectrum and photovoltaic property seem at odds; i.e., the photovoltaic response often decreases as the absorption wavelength increases, especially in the NIR spectral region.^{15–17} There must be a compromise or trade-off between the response range and device performance. On the other hand, for the most widely used bulk heterojunction (BHJ) structure of organic photovoltaic devices, in which the electron donor and acceptor (usually fullerene derivatives) materials are mixed together, an offset of larger than 0.3 eV between the lowest unoccupied molecular orbital (LUMO) energy levels of the polymer donor and fullerene acceptor is needed for efficient exciton separation.^{18–21} To increase the absorption range or decrease the bandgap (E_g), as well as maintain an appropriate LUMO energy level, the highest occupied molecular orbital (HOMO) energy level must shift upward.^{22,23} All these demands should be carefully considered and manipulated through molecular design and synthesis. Thus, a suitable polymer for UV–vis–NIR light detection should possess the characteristics of broad

Received: April 24, 2015

Revised: June 2, 2015

Published: June 11, 2015

absorption, proper energy levels, and optimized thin-film property.

The construction of donor–acceptor (D–A) or push–pull chain architecture, in which electron-rich and electron-deficient units are alternately arranged along the polymer backbone, is a common approach to achieving the desirable optical bandgaps and energy levels of conjugated polymers.^{24–28} As the acceptors with a large difference in electron-withdrawing strength are more available, it is convenient to tune the absorption profile and energy levels by selection of appropriate electron-deficient groups.^{29,30} Accordingly, incorporation of weak donor and strong acceptor in conjugated polymers usually leads to long and broad absorption, which depends on the electron-withdrawing strength.^{31–37} For example, Wudl et al. reported that using a weak donor of dithiophene and a strong acceptor of benzobisthiadiazole (BBT), a polymer exhibited long and broad absorption and high carrier mobility.³¹ Andersson et al. reported the use of thiophene as a weak donor and thiadiazoloquinoxaline (TQ) as a strong acceptor to construct a polymer that had a maximal absorption at 1400 nm and very broad absorption up to 2000 nm.³² In the work reported by Fréchet et al., when increasing the electron deficiency from isoindigo (IIG) to thienobenzoisoindigo (TBIIG) and to thienoisooindigo (TIIG), the maximal absorption peaks of the corresponding D–A polymers shifted significantly to the long wavelength, and the full width at half-maxima (fwhm) also broadened greatly. Likewise, the energy levels and film properties were influenced as well, leading to different photovoltaic and field-effect properties.³³ Nevertheless, it seems that most of the ultralow-bandgap polymers do not exhibit satisfied photovoltaic response, and little solar cell performance has been reported. One possible reason may be due to that the bandgaps and energy levels have not been tuned precisely. Recently, random D–A copolymers, consisting of one electron-rich unit and two electron-deficient units with different electron-withdrawing properties, were prepared for use in organic photovoltaic devices.^{38–42} The main advantages of multiple-component D–A copolymers include broad absorption, finely tuned energy levels, and adjustable thin-film properties, which are deemed to be highly beneficial for the development of panchromatic photodetectors.

Herein, we report the synthesis of a series of donor–acceptor copolymers, using thiophene as a weak donor and diketopyrrolopyrrole (DPP) and thienoisooindigo (TIIG) as acceptors with different electron-withdrawing strength. Variation in the two acceptor ratios in copolymers affects the electronic energy levels, absorption profile, and thin-film property and as well device performance. The molecular structure–material property–device performance relationships are established with these copolymers.

EXPERIMENTAL SECTION

Materials. All the chemicals and reagents were purchased from commercial sources and used as received. The solvents for chemical syntheses were purified by distillation. Chemical reactions were carried out under an argon atmosphere. Detailed syntheses and characterizations of the monomers and polymers are given in the Supporting Information.

Characterizations. The nuclear magnetic resonance (NMR) spectra were recorded on a Bruker Avance 400 NMR spectrometer. Matrix-assisted laser desorption ionization time-of-flight mass spectrometry (MALDI-TOF MS) was obtained from Bruker Daltonics Autoflex III TOF/TOF. Thermogravimetric analysis (TGA) was done on a PerkinElmer Pyris Diamond TG from 50 to 800 °C at a heating

rate of 10 °C/min under a continuous nitrogen flow. Differential scanning calorimetry (DSC) was performed on a TA-DSC Q100 from 20 to 280 °C with a heating/cooling rate of 10 °C/min under a nitrogen atmosphere. Gel permeation chromatography (GPC) analysis was conducted on a Waters 2414 system with polystyrene (PS) as standard and chloroform as eluent at room temperature. The UV-vis–NIR absorption spectra were recorded on a Shimadzu UV-3600 spectrophotometer. Cyclic voltammetry (CV) was performed on a CHI660b electrochemical workstation in a solution of *n*-Bu₄NPF₆ (0.1 M) in dry acetonitrile with a scan rate of 50 mV/s at room temperature under an argon atmosphere. A Pt disk (2 mm diameter) was used as the working electrode with a Pt wire as the counter electrode and an Ag/AgCl electrode as the reference electrode. The redox potentials were calibrated by using ferrocene as an internal standard. The out-of-plane and in-plane grazing incidence X-ray diffraction (GIXRD) profiles were performed using a Rigaku SmartLab X-ray diffractometer equipped with Cu target, CBO mirror, thin film sample stage, and a scintillation detector. The scan rate was in 0.05° step size (2θ) and 5 s per step. Atomic force microscopy (AFM) studies were carried out on a SPA300HV instrument equipped with a SPI3800N controller (Seiko Instruments, Japan) in tapping mode in ambient condition using silicon cantilevers (Applied Nanostructures, nominal spring constant of 2.0 N/m and nominal resonance frequency of ~75 kHz).

Fabrication of Photodetectors. A mixture of a given polymer and [6,6]-phenyl-C₇₁-butyric acid methyl ester (PCBM, ADS71BFA) in a weight ratio of 1:2 was dissolved in chloroform (in the optimized device, 3% DIO in volume was added as the additive) with a total concentration of 18 mg/mL and stirred under a nitrogen atmosphere at room temperature for more than 12 h. For device fabrication, patterned indium tin oxide (ITO) glass substrates were cleaned, sequentially, by ultrasonic treatment in detergent, deionized water, acetone, and isopropyl alcohol, then dried in an oven at 110 °C for 1 h, and treated with UV-plasma for 15 min. PEDOT:PSS (Baytron P VP A1 4083) was spin-coated at 3500 rpm for 60 s and dried at 110 °C for 30 min, forming a film of about 30 nm thickness. Subsequently, the active layer was prepared by spin-coating at a speed of 1000 rpm for 60 s in a nitrogen-filled glovebox to get a film of 190 nm thickness. 10 nm of BCP and 100 nm of Al electrode were successively deposited by thermal evaporation using a shadow mask (the active area is 0.16 cm²).

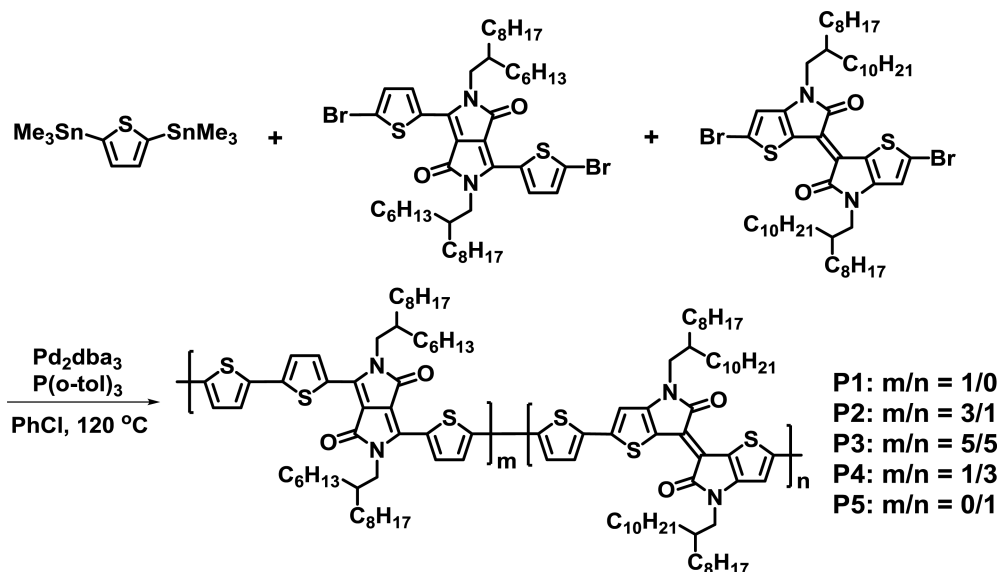
Characterization of Photodetectors. EQE measurements were conducted under ambient conditions in air using an EQE system from Beijing 7-Star Optical Instruments Co., Ltd. Incident light from a 250 W halogen lamp which passed through two cascade monochromators was chopped at 25 Hz and focused on the active area of the device. The photocurrent signal was first amplified using a low-noise current amplifier (DLPCA-200, Femto) and then detected with a lock-in amplifier (SR830, Stanford Research Systems). We used a Keithley 236 Source Measure unit to measure the dark current density–voltage (*J*–*V* curve) characteristics of the devices.

RESULTS AND DISCUSSION

Synthesis and Characterization. Among many electron-deficient compounds being developed for use in D–A type polymers,^{43–45} DPP and TIIG have been widely used in making low-bandgap polymers, as they all possess high absorption coefficient, good film-forming property, and high carrier mobility,^{46–49} while they also exhibit some different properties, for example, complementary absorption profiles and different electrochemical properties.^{50,51} Thus, copolymers containing these two acceptor units may show long and broad absorption characteristics, tunable energy levels and bandgaps, and other characteristics desirable for improving the performance of polymer photodetectors.

The monomers were synthesized according to the procedures in the literature, and the characterizations are presented in the Supporting Information.^{46,48} The polymerization was carried out via the Stille cross-coupling reaction of

Scheme 1. Synthesis of Polymers P1–P5



three monomers in different mole ratios (Scheme 1). The resulting polymers are readily soluble in common organic solvents such as chloroform, toluene, and chlorobenzene. The elemental analysis results of the polymers match well with theoretical values, which confirms that the copolymers are related to the monomers in feed. The molecular weights of the polymers were measured by gel permeation chromatography (GPC). The number-average molecular weights (M_n) of the polymers are around 20–30 kDa, and the polydispersity indexes (PDI) are between 2.0 and 2.5 (Table 1). Thermal

noticeable change in color (Figure 1). Interestingly, the fwhm of the low-energy absorption bands become broader from **P1** to **P5** (233, 269, 346, 376, and 393 nm), which is deemed to be beneficial for realizing UV-vis-NIR photoresponse.

Cyclic voltammetry (CV) was used to determine the energy levels of the polymers (Figure S3). From the onset oxidation ($E_{\text{on}}^{\text{ox}}$) and reduction potentials ($E_{\text{on}}^{\text{red}}$), the HOMO and LUMO energy levels are calculated according to the equations $E_{\text{HOMO}} = -e(E_{\text{on}}^{\text{ox}} + 4.43)$ and $E_{\text{LUMO}} = -e(E_{\text{on}}^{\text{red}} + 4.43)$. The HOMO energy levels of **P1–P5** are -5.41 , -5.12 , -5.02 , -4.87 , and -4.76 eV, respectively, while the LUMO energy levels of all the polymers are calculated to be around -3.6 eV (Table 2). As the content of TIIG acceptor increases, the LUMO energy levels remain unchanged but the HOMO energy levels increase in steps, thereby reducing the bandgaps. Schematic diagrams of the energy levels (Figure 2) imply an efficient charge transfer from the polymers to PCBM.^{19,20}

Molecular Stacking and Morphology. X-ray diffraction (XRD) analysis was done to study the effect of structural changes on the polymer stacking. Figures 3a and 3b show the out-of-plane and in-plane grazing incidence X-ray diffraction (GIXRD) patterns of polymer films spin-coated on quartz substrate. The diffraction peaks at small and large 2θ zone can be ascribed to the laminar packing and $\pi-\pi$ stacking between polymer backbones, respectively.^{52,53} The laminar diffraction peaks of **P1–P5** are at 4.35 , 4.05 , 3.85 , 3.70 , and 3.55° , corresponding to d -spacing of 2.03 , 2.18 , 2.29 , 2.39 , and 2.49 nm, respectively. Interestingly, the diffraction intensity of the laminar packing increases from **P1** to **P5** in the in-plane GIXRD, while the corresponding values in the out-of-plane diagrams decrease. In the out-of-plane GIXRD diagrams, the $\pi-\pi$ diffraction peaks of **P1–P5** at 23.70 , 23.85 , 23.95 , 24.05 , and 24.30° are associated with d -spacing of 3.75 , 3.73 , 3.71 , 3.70 , and 3.66 Å, and there are no related peaks observed in the in-plane GIXRD. These results indicate that with the increase of TIIG content in polymers the face-on orientation is preferred.⁵⁴

In order to gain in-depth insight into the film nanostructure, atomic force microscopy (AFM) was used to investigate the surface morphology of polymer films. As shown in Figure 3c, the root-mean-square (RMS) roughness of the pristine films of

Table 1. Characterizations of Polymers P1–P5

polymer	TIIG (%)	M_n (kDa)	M_w (kDa)	PDI	T_d^a (°C)
P1	0	28	67	2.4	401
P2	25	31	78	2.5	395
P3	50	24	57	2.4	392
P4	75	26	59	2.3	391
P5	100	26	53	2.0	397

^aOnset temperatures of 5% weight loss in nitrogen from TGA traces.

properties of these polymers were analyzed by thermogravimetric analysis (TGA) and differential scanning calorimetry (DSC) (Table 1 and Supporting Information). The decomposition temperatures (T_d) as measured for 5% loss weight in nitrogen are above 390 °C, indicating good thermal stability and adequate for electronic device application. The polymers also exhibit good stability under ambient conditions in air for more than 5 months. There are no apparent thermal transitions in the second heating and cooling DSC scans for all the polymers.

Optical and Electrochemical Property. The UV-vis-NIR absorption spectra of the polymers in dilute chloroform and as thin films spin-coated on quartz are shown in Figure 1. All the polymers show similar intense and broad absorption profiles, with a maximal peak between 824 and 993 nm. The maximal and onset absorptions of the films of **P1** to **P5** gradually red-shifts as the content of more electron-deficient acceptor of TIIG unit increases, representing the optical bandgap (E_g^{opt}) tuning from 1.34 to 0.96 eV (Table 2). At the same time, the polymer solutions and films also display a

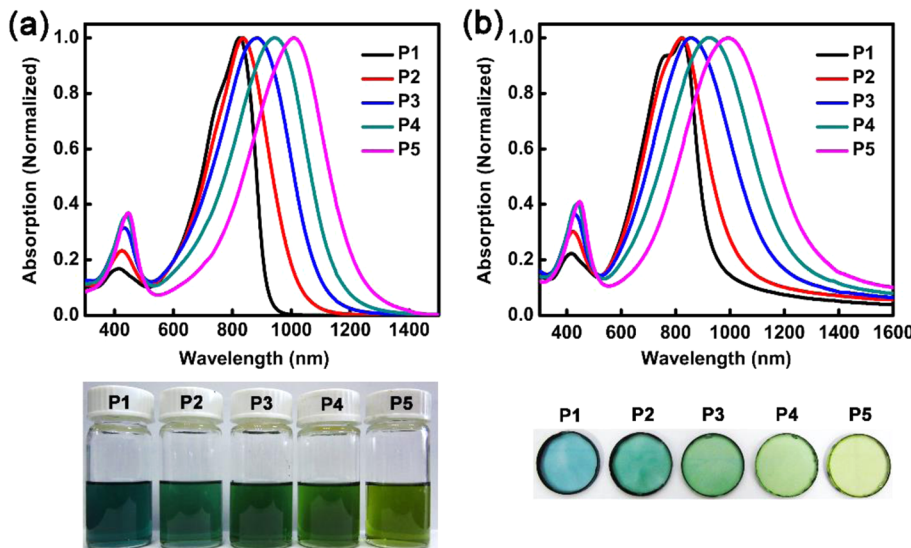


Figure 1. Absorption spectra of the polymers (a) in dilute chloroform (at a concentration of 0.03 g/L) and (b) as films spin-coated on quartz. The photographs of the polymer solutions and films are shown below.

Table 2. Optical and Electrochemical Properties of Polymers P1–P5

polymer	$\lambda_{\text{max}}^{\text{soln}} \text{ } ^a$ (nm)	$\lambda_{\text{max}}^{\text{film}} \text{ } ^b$ (nm)	fwhm ^c (nm)	$E_g^{\text{opt}} \text{ } ^d$ (eV)	HOMO ^e (eV)	LUMO ^e (eV)	$E_g^{\text{EC}} \text{ } ^f$ (eV)
P1	825	824	233	1.34	-5.41	-3.61	1.80
P2	836	823	269	1.22	-5.12	-3.59	1.53
P3	886	857	346	1.08	-5.02	-3.61	1.41
P4	943	924	376	1.01	-4.87	-3.57	1.30
P5	1009	993	393	0.96	-4.76	-3.60	1.16

^aMeasured in chloroform at a concentration of 0.03 g/L. ^bFilm spin-cast from 10 mg/mL chloroform solution on quartz substrate. ^cThe full width at half-maxima (fwhm) of the film absorption spectra. ^dOptical bandgap (estimated from the film absorption onset). ^eCalculated from $E_{\text{LUMO}} = -e(E_{\text{on}}^{\text{red}} + 4.43)$ and $E_{\text{HOMO}} = -e(E_{\text{on}}^{\text{ox}} + 4.43)$. ^fElectrochemical band gap is derived from E_{HOMO} subtracting E_{LUMO} .

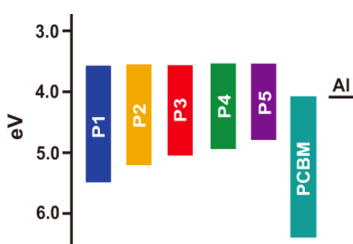


Figure 2. Energy level diagrams of polymers P1–P5 relative to PCBM and Al.

P1–P5 are 0.66, 0.81, 0.51, 0.54, and 0.87 nm, respectively. The polymer films exhibit similar nanoscale morphology and have good-quality and smooth surfaces.

Photodetector Performance. The photodetector was fabricated in a BHJ structure with a device architecture of ITO/PEDOT:PSS/active layer/BCP/Al. The active layer consists of a given polymer and PC₇₁BM in a 1:2 weight ratio. To minimize the dark current, a thin layer of 2,9-dimethyl-4,7-diphenyl-1,10-phenanthroline (BCP) was inserted between the active layer and aluminum electrode to suppress charge injection from the cathode to the active layer.^{55,56} The devices (basic device) performed poorly when the active layer was processed using chloroform as the solvent. When using 3% 1,8-diiodooctane (DIO) as the additive in solvent for film coating, the devices (optimized device) showed significant improvement in performance (Figure 4 and Table 3). The prodigious variation in device performance is possibly

attributed to changes in the film morphology brought by the DIO additive.^{57–59}

The current density–voltage (J – V) characteristics of all the devices (Supporting Information) show a typical rectification behavior, indicating that the photodetectors have the asymmetry characteristics. The dark current increases from the devices fabricated with P1 to P5, and the relevant diode property decreases. The reason for this phenomenon is likely that the HOMO energy levels shift upward with increased TIIG composition, which facilitates charge injection from the cathode to the active layer.^{60,61} The difference in dark J – V curves may be related to the energy difference between the HOMO of the polymers and the LUMO of PCBM.^{6,62} Comparing the dark current of the basic and optimized devices, we find that the dark current decreases for about 1 order of magnitude after the addition of DIO. Thus, the energy levels and film morphology can affect the dark current of organic photodetectors.

If we assume that the shot noise from dark current is the major contributor to the noise,^{6,9,55,63} the figure-of-merit for a photodetector or specific detectivity (D^*) can be expressed as

$$D^* = R/(2qJ_d)^{1/2} = (J_{\text{ph}}/J_{\text{light}})/(2qJ_d)^{1/2} \text{ (Jones)}$$

where R is the responsivity, a ratio of photocurrent (J_{ph}) to incident-light intensity (J_{light}), q is the absolute value of electron charge (1.6×10^{-19} C), and J_d is the dark current density (A/cm^2). Accordingly, the D^* values of the photodetectors based on polymers P1–P5 are calculated and shown in Figure 4 and Table 3. It is found that going from P1 to P5, the highest

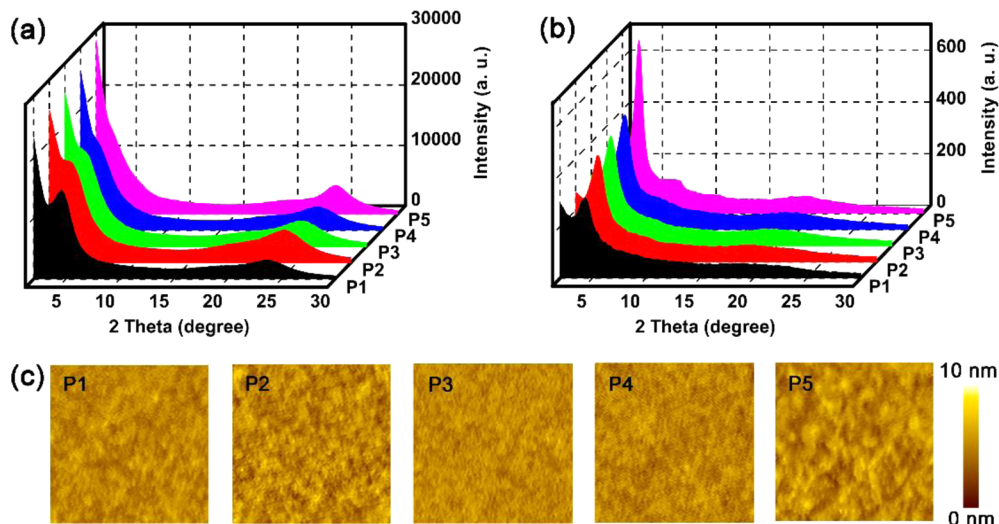


Figure 3. (a) Out-of-plane and (b) in-plane GIXRD diagrams and (c) AFM height images ($1 \mu\text{m} \times 1 \mu\text{m}$) of the pristine polymer films spin-coated on quartz substrate.

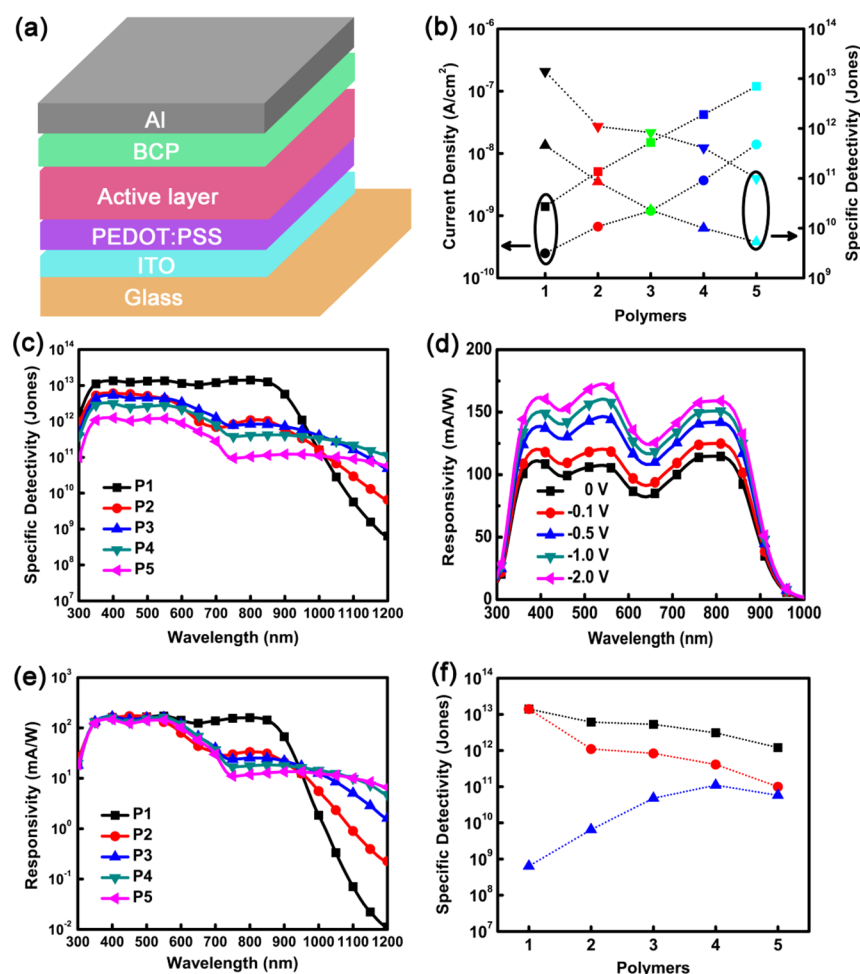


Figure 4. (a) Schematic device structure. (b) Dark current density and specific detectivity of the basic and optimized devices based on P1–P5 at 800 nm under -0.1 V . (c) Spectral specific detectivity of the optimized devices based on P1–P5 under -0.1 V . (d) Spectral responsivity of the optimized photodetector fabricated with P1 under different voltages. (e) Spectral responsivity of the optimized devices based on P1–P5 under -2.0 V . (f) Specific detectivity of the optimized devices fabricated with P1–P5 at 400 nm (black square), 800 nm (red circle) and 1200 nm (blue up-triangle) under -0.1 V .

specific detectivity of the photodetectors decreases, while the response range increases. As a result, the optimized device

based on P1 exhibits the highest specific detectivity of 1.4×10^{13} Jones at 800 nm under -0.1 V , while the device based on

Table 3. Characteristics of the Basic and Optimized Devices

polymer	basic device			optimized device		
	R^a (mA/W)	J_d^b (A/cm ²)	D^{*b} (Jones)	R^a (mA/W)	J_d^b (A/cm ²)	D^{*b} (Jones)
P1	20.8	1.4×10^{-9}	4.6×10^{11}	159.0	2.5×10^{-10}	1.4×10^{13}
P2	4.3	5.1×10^{-9}	8.5×10^{10}	33.4	6.7×10^{-10}	1.1×10^{12}
P3	2.4	1.5×10^{-8}	2.3×10^{10}	25.2	1.2×10^{-9}	8.3×10^{11}
P4	2.2	4.2×10^{-8}	1.0×10^{10}	17.8	3.7×10^{-9}	4.1×10^{11}
P5	1.8	1.2×10^{-7}	5.3×10^9	11.9	1.4×10^{-8}	1.0×10^{11}

^aResponsivity at 800 nm under -2 V. ^bDark current density and specific detectivity at 800 nm under -0.1 V.

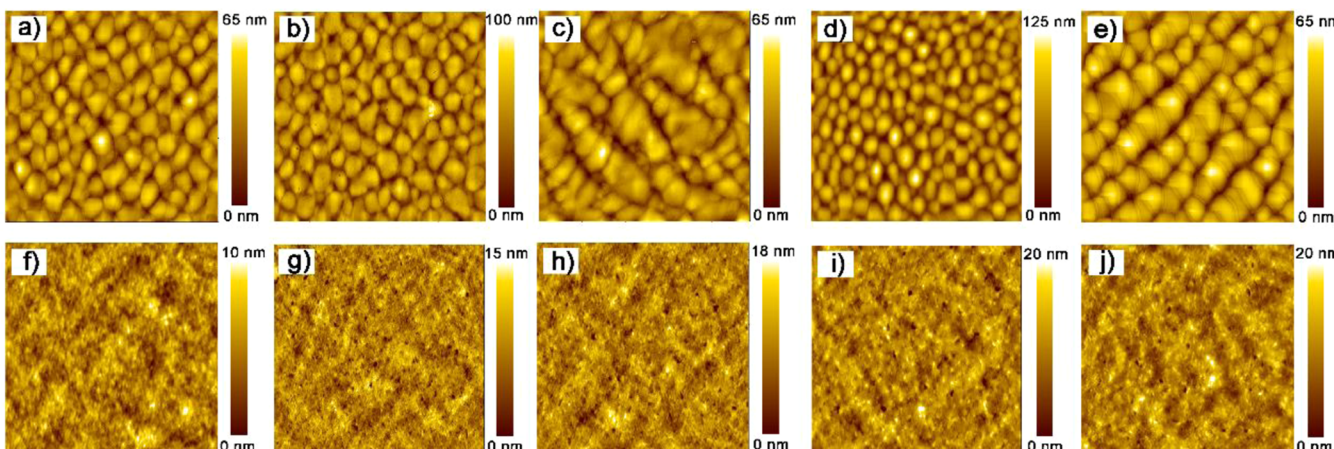


Figure 5. AFM topography images of the BHJ active layers spin-coated on glass/ITO/PEDOT:PSS using chloroform (a–e for P1–P5, 5 μm × 5 μm) and chloroform with 3% DIO (f–j for P1–P5, 2 μm × 2 μm) as the solvents.

P5 shows the most broad response of 300–1200 nm. The results are among the best performance for UV-vis-NIR polymer photodetectors. Spectral responsivity of the optimized photodetector fabricated with P1 appears to be voltage-dependent (Figure 4d), which is likely due to the field-induced charge transport and injection.^{64,65} Similarly, the responsivity and specific detectivity of other devices also depend on the electric field (Supporting Information).

The photodetector based on P1 performs better than others in the UV-vis spectral region. However, due to the relatively wide bandgap, the response of P1 in NIR spectral region is limited. The other polymers show better response in low-energy spectral region as the narrower bandgaps. As shown in Figure 4e and Supporting Information, responsivities of all the optimized devices at 400 nm under -2 V (R_{400}) are nearly the same, while the data at 800 nm (R_{800}) sharply decrease from the devices with P1 to P2 and then gradually decrease to P5. On the other hand, the responsivity at 1200 nm (R_{1200}) increase from P1 to P5, as the absorption at 1200 nm increase in the same order (Figure S4). According to the equation mentioned above, the specific detectivity is not only determined by the responsivity but also influenced by the dark current. The different responsivity and dark current result in diverse values of D^* . The specific detectivity of the optimized devices at the wavelength of 400, 800, and 1200 nm are depicted in Figure 4f and Table S1. The specific detectivity at 400 nm (D_{400}^*) and 800 nm (D_{800}^*) under -0.1 V decrease from P1 to P5, while the values at 1200 nm (D_{1200}^*) increase from P1 to P4 and slightly decrease with P5. As a result, the optimized photodetectors based on P3 and P4 exhibit the merit of both broad response and high detectivity, rendering the importance of bandgap optimization.

Film Morphology. It is well-known that the device performance of polymer solar cells and photodetectors is closely related to the active layer morphology.^{66,67} The appropriate nanoscale topography is critically important for good photovoltaic response. The surface topography of the active layer was then investigated by tapping-mode AFM in order to probe any changes in the film morphology brought by the use of DIO additive. As shown in Figure 5, the BHJ films of the basic and optimized devices exhibit rather different morphology. Without the use of DIO, large domains of hundreds of nanometers are observed in the film, while the domain sizes decrease dramatically for the film processed with chloroform containing 3% DIO additive. It was reported that a small domain size of tens of nanometers is the most favorable for exciton separation and charge transport, which could explain the high responsivity and low dark current in the optimized devices.^{68,69} Our results clearly indicate that the active layer morphology can critically affect the performance of polymer photodetectors, in particular the spectral responsivity and dark current.

CONCLUSION

We have demonstrated that the use of a weak donor and two strong acceptors in copolymers is an effective approach to achieving broad response and high detectivity of polymer photodetectors. By adjusting the ratio of the two acceptors of DPP and TIIG in copolymers, the ideal properties such as absorption profile, energy levels, and molecular stacking can be obtained, which lead to the broad spectral responsivity and low dark current of the photodetector. The molecular structure–material property–device performance relationships are established with these copolymers. The photodetector based on P4

exhibits specific detectivity of greater than 10^{11} Jones in a broad spectral region of 300–1200 nm, which is really promising for UV-vis–NIR light detection.

■ ASSOCIATED CONTENT

§ Supporting Information

TGA, DSC, and CV traces of the polymers, absorption spectra of the mixed films of polymers P1–P5, and PCBM and device characterizations (dark J – V curves, spectral responsivity, and specific detectivity) as well as syntheses and characterizations of the monomers and polymers. The Supporting Information is available free of charge on the ACS Publications website at DOI: 10.1021/acs.macromol.5b00859.

■ AUTHOR INFORMATION

Corresponding Authors

*E-mail wqqiao@ciac.ac.cn (W.Q.).

*E-mail wayne_wang@carleton.ca (Z.Y.W.).

Notes

The authors declare no competing financial interest.

■ ACKNOWLEDGMENTS

This work was supported by National Natural Science Foundation of China (21134005, 21474102, 21474105, and U1332116) and the Natural Science and Engineering Research Council of Canada.

■ REFERENCES

- Konstantatos, G.; Howard, I.; Fischer, A.; Hoogland, S.; Clifford, J.; Klem, E.; Levina, L.; Sargent, E. H. *Nature* **2006**, *442*, 180–183.
- Sargent, E. H. *Nat. Photonics* **2009**, *3*, 325–331.
- Rauch, T.; Böberl, M.; Tedde, S. F.; Fürst, J.; Kovalenko, M. V.; Hesser, G.; Lemmer, U.; Heiss, W.; Hayden, O. *Nat. Photonics* **2009**, *3*, 332–336.
- Clifford, J. P.; Konstantatos, G.; Johnston, K. W.; Hoogland, S.; Levina, L.; Sargent, E. H. *Nat. Nanotechnol.* **2009**, *4*, 40–44.
- Clark, J.; Lanzan, G. *Nat. Photonics* **2010**, *4*, 438–446.
- Gong, X.; Tong, M.; Xia, Y.; Cai, W.; Moon, J. S.; Cao, Y.; Yu, G.; Shieh, C.-L.; Nilsson, B.; Heeger, A. J. *Science* **2009**, *325*, 1665–1667.
- Dong, H.; Zhu, H.; Meng, Q.; Gong, X.; Hu, W. *Chem. Soc. Rev.* **2012**, *41*, 1754–1808.
- Saracco, E.; Bouthinon, B.; Verilhac, J.-M.; Celle, C.; Chevalier, N.; Mariolle, D.; Dhez, O.; Simonato, J.-P. *Adv. Mater.* **2013**, *25*, 6534–6538.
- Qi, J.; Zhou, X.; Yang, D.; Qiao, W.; Ma, D.; Wang, Z. Y. *Adv. Funct. Mater.* **2014**, *24*, 7605–7612.
- Dong, R.; Bi, C.; Dong, Q.; Guo, F.; Yuan, Y.; Fang, Y.; Xiao, Z.; Huang, J. *Adv. Opt. Mater.* **2014**, *2*, 549–554.
- Yao, Y.; Liang, Y.; Shrotriya, V.; Xiao, S.; Yu, L.; Yang, Y. *Adv. Mater.* **2007**, *19*, 3979–3983.
- Chen, E.-C.; Tseng, S.-R.; Chao, Y.-C.; Meng, H.-F.; Wang, C.-F.; Chen, W.-C.; Hsu, C.-S.; Horng, S.-F. *Synth. Met.* **2011**, *161*, 1618–1622.
- Liu, X.; Wang, H.; Yang, T.; Zhang, W.; Gong, X. *ACS Appl. Mater. Interfaces* **2012**, *4*, 3701–3705.
- Liu, X.; Wang, H.; Yang, T.; Zhang, W.; Hsieh, I.-F.; Cheng, S. Z. D.; Gong, X. *Org. Electron.* **2012**, *13*, 2929–2934.
- Chen, L.; Deng, D.; Nan, Y.; Shi, M.; Chan, P. K. L.; Chen, H. J. *Phys. Chem. C* **2011**, *115*, 11282–11292.
- Keshtova, M. L.; Marochkina, D. V.; Fu, Y.; Xie, Z.; Geng, Y.; Kochurov, V. S.; Khokhlov, A. R. *Chin. J. Polym. Sci.* **2014**, *32*, 844–853.
- Qian, G.; Qi, J.; Wang, Z. Y. *J. Mater. Chem.* **2012**, *22*, 12867–12873.
- Yu, G.; Gao, J.; Hummelen, J. C.; Wudl, F.; Heeger, A. J. *Science* **1995**, *270*, 1789–1791.
- Blom, P. W. M.; Mihailetti, V. D.; Koster, L. J. A.; Markov, D. E. *Adv. Mater.* **2007**, *19*, 1551–1566.
- Li, G.; Zhu, R.; Yang, Y. *Nat. Photonics* **2012**, *6*, 153–161.
- Sun, S.-S. *Sol. Energy Mater. Sol. Cells* **2005**, *85*, 261–267.
- Li, Y. *Acc. Chem. Res.* **2012**, *45*, 723–733.
- Chao, Y.-H.; Jheng, J.-F.; Wu, J.-S.; Wu, K.-Y.; Peng, H.-H.; Tsai, M.-C.; Wang, C.-L.; Hsiao, Y.-N.; Wang, C.-L.; Lin, C.-Y.; Hsu, C.-S. *Adv. Mater.* **2014**, *26*, 5205–5210.
- Lei, T.; Dou, J.-H.; Ma, Z.-J.; Yao, C.-H.; Liu, C.-J.; Wang, J.-Y.; Pei, J. *J. Am. Chem. Soc.* **2012**, *134*, 20025–20028.
- Huang, Y.; Guo, X.; Liu, F.; Huo, L.; Chen, Y.; Russell, T. P.; Han, C. C.; Li, Y.; Hou, J. *Adv. Mater.* **2012**, *24*, 3383–3389.
- Cui, C.; Wong, W.-Y.; Li, Y. *Energy Environ. Sci.* **2014**, *7*, 2276–2284.
- Chu, T.-Y.; Lu, J.; Beaupré, S.; Zhang, Y.; Pouliot, J.-R.; Zhou, J.; Najari, A.; Leclerc, M.; Tao, Y. *Adv. Funct. Mater.* **2012**, *22*, 2345–2351.
- Cui, W.; Wudl, F. *Macromolecules* **2013**, *46*, 7232–7238.
- Wang, Z. Y. *Near-Infrared Organic Materials and Emerging Applications*; CRC Press: Boca Raton, FL, 2013; Chapter 4.
- Yuen, J. D.; Wudl, F. *Energy Environ. Sci.* **2013**, *6*, 392–406.
- Fan, J.; Yuen, J. D.; Cui, W.; Seifter, J.; Mohebbi, A. R.; Wang, M.; Zhou, H.; Heeger, A. J.; Wudl, F. *Adv. Mater.* **2012**, *24*, 6164–6168.
- Steckler, T. T.; Henriksson, P.; Mollinger, S.; Lundin, A.; Salleo, A.; Andersson, M. R. *J. Am. Chem. Soc.* **2014**, *136*, 1190–1193.
- Chen, M. S.; Niskala, J. R.; Unruh, D. A.; Chu, C. K.; Lee, O. P.; Fréchet, J. M. *J. Chem. Mater.* **2013**, *25*, 4088–4096.
- Yau, C. P.; Fei, Z.; Ashraf, R. S.; Shahid, M.; Watkins, S. E.; Pattanasattayavong, P.; Anthopoulos, T. D.; Gregoriou, V. G.; Chochos, C. L.; Heaney, M. *Adv. Funct. Mater.* **2014**, *24*, 678–687.
- Zhang, X.; Steckler, T. T.; Dasari, R. R.; Ohira, S.; Potsavage, W. J., Jr.; Tiwari, S. P.; Coppée, S.; Ellinger, S.; Barlow, S.; Brédas, J.-L.; Kippelen, B.; Reynolds, J. R.; Marder, S. R. *J. Mater. Chem.* **2010**, *20*, 123–134.
- Zhou, H.; Yang, L.; Stoneking, S.; You, W. *ACS Appl. Mater. Interfaces* **2012**, *4*, 3701–3705.
- Kuramochi, M.; Kuwabara, J.; Lu, W.; Kanbara, T. *Macromolecules* **2014**, *47*, 7378–7385.
- Jung, J. W.; Liu, F.; Russell, T. P.; Jo, W. H. *Energy Environ. Sci.* **2013**, *6*, 3301–3307.
- Kang, T. E.; Cho, H.-H.; jun Kim, H.; Lee, W.; Kang, H.; Kim, B. *J. Macromolecules* **2013**, *46*, 6806–6813.
- Jiang, J.-M.; Chen, H.-C.; Lin, H.-K.; Yu, C.-M.; Lan, S.-C.; Liu, C.-M.; Wei, K.-H. *Polym. Chem.* **2013**, *4*, 5321–5328.
- Burkhart, B.; Khlyabich, P. P.; Thompson, B. C. *ACS Macro Lett.* **2012**, *1*, 660–666.
- Zhou, J.; Xie, S.; Amond, E. F.; Becker, M. L. *Macromolecules* **2013**, *46*, 3391–3394.
- Pron, A.; Leclerc, M. *Prog. Polym. Sci.* **2013**, *38*, 1815–1831.
- Kroon, R.; de Z. Mendaza, A. D.; Himmelberger, S.; Bergqvist, J.; Bäcke, O.; Faria, G. C.; Gao, F.; Obaid, A.; Zhuang, W.; Gedefaw, D.; Olsson, E.; Inganäs, O.; Salleo, A.; Müller, C.; Andersson, M. R. *J. Am. Chem. Soc.* **2014**, *136*, 11578–11581.
- Li, Y.; Sonar, P.; Murphy, L.; Hong, W. *Energy Environ. Sci.* **2013**, *6*, 1684–1710.
- Mei, J.; Kim, D. H.; Ayzner, A. L.; Toney, M. F.; Bao, Z. *J. Am. Chem. Soc.* **2011**, *133*, 20130–20133.
- Sun, B.; Hong, W.; Yan, Z.; Aziz, H.; Li, Y. *Adv. Mater.* **2014**, *26*, 2636–2642.
- Dutta, G. K.; Han, A.-R.; Lee, J.; Kim, Y.; Oh, J. H.; Yang, C. *Adv. Funct. Mater.* **2013**, *23*, 5317–5325.
- Kim, G.; Kang, S.-J.; Dutta, G. K.; Han, Y.-K.; Shin, T. J.; Noh, Y.-Y.; Yang, C. *J. Am. Chem. Soc.* **2014**, *136*, 9477–9483.
- Li, W.; Roelofs, W. S. C.; Wienk, M. M.; Janssen, R. A. J. *J. Am. Chem. Soc.* **2012**, *134*, 13787–13795.
- Koizumi, Y.; Ide, M.; Saeki, A.; Vijayakumar, C.; Balan, B.; Kawamoto, M.; Seki, S. *Polym. Chem.* **2013**, *4*, 484–494.

- (52) Ashraf, R. S.; Kronemeijer, A. J.; James, D. I.; Sirringhaus, H.; McCulloch, I. *Chem. Commun.* **2012**, *48*, 3939–3941.
- (53) Wang, Q.; Zhang, S.; Ye, L.; Cui, Y.; Fan, H.; Hou, J. *Macromolecules* **2014**, *47*, 5558–5565.
- (54) Wu, Y.; Li, Z.; Ma, W.; Huang, Y.; Huo, L.; Guo, X.; Zhang, M.; Ade, H.; Hou, J. *Adv. Mater.* **2013**, *25*, 3449–3455.
- (55) Guo, F.; Yang, B.; Yuan, Y.; Xiao, Z.; Dong, Q.; Bi, Y.; Huang, J. *Nat. Nanotechnol.* **2012**, *7*, 798–802.
- (56) Qi, J.; Ni, L.; Yang, D.; Zhou, X.; Qiao, W.; Li, M.; Ma, D.; Wang, Z. Y. *J. Mater. Chem. C* **2014**, *2*, 2431–2438.
- (57) Lee, J. K.; Ma, W. L.; Brabec, C. J.; Yuen, J.; Moon, J. S.; Kim, J. Y.; Lee, K.; Bazan, G. C.; Heeger, A. J. *J. Am. Chem. Soc.* **2008**, *130*, 3619–3623.
- (58) Kramer, E. J.; Heeger, A. J.; Bazan, G. C. *Chem. Rev.* **2014**, *114*, 7006–7043.
- (59) Li, G.; Kang, C.; Gong, X.; Zhang, J.; Li, C.; Chen, Y.; Dong, H.; Hu, W.; Li, F.; Bo, Z. *Macromolecules* **2014**, *47*, 4645–4652.
- (60) Baeg, K.-J.; Bindra, M.; Natali, D.; Caironi, M.; Noh, Y.-Y. *Adv. Mater.* **2013**, *25*, 4267–4295.
- (61) Braun, S.; Salaneck, W. R.; Fahlman, M. *Adv. Mater.* **2009**, *21*, 1450–1472.
- (62) Giebink, N. C.; Wiederrecht, G. P.; Wasielewski, M. R.; Forrest, S. R. *Phys. Rev. B* **2010**, *82*, 155305.
- (63) Qian, G.; Qi, J.; Davey, J. A.; Wright, J. S.; Wang, Z. Y. *Chem. Mater.* **2012**, *24*, 2364–2372.
- (64) Yang, D.; Xu, K.; Zhou, X.; Wang, Y.; Ma, D. *J. Appl. Phys.* **2014**, *115*, 244506.
- (65) Qi, J.; Gao, Y.; Zhou, X.; Yang, D.; Qiao, W.; Ma, D.; Wang, Z. Y. *Adv. Mater. Interfaces* **2015**, *2*, 1400475.
- (66) Keivanidis, P. E.; Ho, P. K. H.; Friend, R. H.; Greenham, N. C. *Adv. Funct. Mater.* **2010**, *20*, 3895–3903.
- (67) Chung, D. S.; Rho, Y.; Ree, M.; Kwon, S.-K.; Kim, Y.-H. *ACS Appl. Mater. Interfaces* **2012**, *4*, 4758–4763.
- (68) Loser, S.; Bruns, C. J.; Miyauchi, H.; Ortiz, R. P.; Facchetti, A.; Stupp, S. I.; Marks, T. J. *J. Am. Chem. Soc.* **2011**, *133*, 8142–8145.
- (69) Chu, T.-Y.; Lu, J.; Beaupré, S.; Zhang, Y.; Pouliot, J.-R.; Wakim, S.; Zhou, J.; Leclerc, M.; Li, Z.; Ding, J.; Tao, Y. *J. Am. Chem. Soc.* **2011**, *133*, 4250–4253.